Anaplastology
ISSN: 2161-1173

Zardawi et al., Anaplastology 2015, 4:1
DOI: 10.4172/2161-1173.1000139

Research Article Open Access

Investigation of Elastomer Infiltration into 3D Printed Facial Soft Tissue Prostheses

Faraedon M Zardawi[1,2], Kaida Xiao[2], Richard van Noort[2] and Julian M Yates[3*]

[1]*Department of Periodontology, School of Dentistry, University of Sulaimani, Iraq*

[2]*Academic Unit of Restorative Dentistry, School of Clinical Dentistry, University of Sheffield, UK*

[3]*Dept of Oral & Maxillofacial Surgery, School of Dentistry, University of Manchester, UK*

***Corresponding author:** Julian M Yates, Professor of Oral & Maxillofacial Surgery, The University of Manchester, Room 1.012 - School of Dentistry, Coupland III Building, Coupland Street, Manchester, M13 9PL, UK, Tel: 0044 (0)1612756865; Fax: 0044 (0)1613061565; E-mail: julian.yates@manchester.ac.uk

Received date: June 04, 2014, **Accepted date:** December 26, 2014, **Published date:** January 1, 2015

Abstract

Objectives: 3D colour printing, a method of additive manufacturing, has been developed and utilised to produce facial soft tissue prostheses. This was achieved by layered fabrication of a biocompatible powder held together by an aqueous binder containing a resin and coloured inks, followed by infiltration with a medical grade silicone polymer. The aim of this study was to investigate the elastomer infiltration depths within the 3D printed models.

Methods: Three sets of 30 cubes – 20x20x20 mm – were used to investigate the infiltration depth of Sil-25 maxillofacial silicone polymer (an MSP) under atmospheric pressure, 2 bar and 3 bar pressure for 5, 10, 15, 20 and 25 min. The investigation was also repeated with two other MSPs – Promax-10 and M-3428 – under 3 bar pressure. Following infiltration, the cubes were bisected, the internal aspects stained with dye, and the infiltration depth measured using a travelling microscope. Infiltration quality was also assessed using scanning electron microscopy (SEM).

Results: At standard atmospheric pressure, the maximum infiltration depth of Sil-25 was 1.45 mm after 25 min. However, after 25 min at 2 and 3 bars pressure, the infiltration depth increased to 3.9 mm and 8.7 mm, respectively. At 3 bars the infiltration depth of Promax-10 and M-3428 was 2.4 mm and 7.5 mm, respectively. In all samples SEM revealed a disorganised distribution of starch particles within the MSP infiltrate.

Significance: Pressure significantly increased the infiltration rate and depth of the MSPs within 3D printed constructs. The infiltration depth obtained is sufficient for prostheses that are less than 16 mm thick.

Keywords: Additive Manufacturing; 3D Colour Printing; Starch Powder; Infiltration; Maxillofacial Silicone Polymer; Sil-25; Scanning Electron Microscopy.

Introduction

Maxillofacial prostheses are constructed to correct facial disfigurement caused by the surgical ablation of cancer, severe facial trauma and congenital craniofacial anomalies [1]. Facial prostheses have been used for many decades to improve aesthetics and function, and to enhance patients' quality of life by improving their psychological condition [2].

The number of patients requiring facial prostheses has increased over the last few decades, primarily due to a general increase in the elderly population and also because of improving cancer survival rates that may or may not involve the facial tissues. Currently, patients in many parts of the world have either no, or limited access to facial prostheses. This is due to a number of reasons including cost, time, technical issues and the availability of highly skilled technicians or anaplastologists required for their fabrication [3]. However, with the development and expansion of rapid prototyping technology, particularly in the production of anatomically accurate human parts [4,5], questions have been raised regarding how best to employ this technique for the rapid manufacturing of facial soft tissue prostheses. Recently, advances have been made in the application of this technology to successfully fabricate accurately fitting facial prostheses with a significantly reduced production time and final product cost [6,7]. Furthermore, these prostheses are biocompatible and of equal quality in terms of texture and colour match. Therefore, the products of this automated technology could have the potential to be available for the majority of patients who require soft tissue facial prostheses worldwide. However, not all aspects of this technology have been fully explored or applied to the field of maxillofacial reconstruction. Laser-scanning techniques, computer-aided design (CAD) and manufacturing (CAM) systems have been used to design and develop auricular prostheses [8,9]. Cheah et al. employed rapid prototyping techniques to fabricate a master pattern "mould" to cast the final prosthesis by integrating laser surface digitizing/scanning and CAD/CAM to achieve automated fabrication of anatomically accurate extra-oral facial prostheses [4,5]. Several techniques have also been reported describing the fabrication of mirror-image wax casts for maxillofacial prostheses [10-14], however it was acknowledged that these techniques are costly and may require more time than manual fabrication. Recently, Eggbeer et al. employed additive manufacturing techniques to undertake the direct manufacture of a body prosthesis from an optical method of data capture, digital design and a 3D

printing process which could then be wrapped in a thin layer of colour-matched silicone elastomer [15], and thus bring the process of utilising rapid prototyping technology in this field one step closer. However, these investigations were not able to fully automate and integrate this technology into practice, as they require the expertise of a maxillofacial technician at key stages to complete the prosthesis.

The use of 3D additive manufacturing technology offers the best possibility for the automated manufacture of facial prostheses. In this project, a seamless, fully automated process was developed and utilised to produce a patient specific (geometry and colour), soft, lightweight and biocompatible soft tissue facial prosthesis (Figure 1).

Figure 1: Photograph of a silicone infiltrated 3D printed powdered construct used to manufacture a bespoke nasal soft tissue prosthesis. Geometry and colour data were translated throughout the CAD/CAM design and manufacturing process.

The project could be summarised as: (1) 3D data capture using a 3D photogrammetry system; (2) manipulation of data in a bespoke 3D CAD package for designing the prostheses; and (3) layered printing using a Z510-3D colour printer.

Due to the fragility of the printed shapes, one key element in this process was the post-production infiltration with a suitable elastomer to provide the printed prostheses with strength and flexibility, and to ensure optimum performance of the printed parts [6,16,17]. The elastomer acted as the main binder for the printed powder, as areas that were not infiltrated became exceedingly fragile as the powder readily disintegrated. In order to achieve optimal performance, it was necessary to obtain optimal infiltration of the elastomers inside the printed powdered construct that was to become the facial prosthesis. Therefore, the aim of the current study was to establish the optimum conditions for infiltration of MSPs into the manufactured powdered constructs. To do this, we evaluated the infiltration depth of three different maxillofacial silicone polymers (MSPs) with different properties; Sil-25, Promax-10 and M3428, inside printed cubes of the same biocompatible powder, under different conditions of pressure and time.

Materials and Methods

Infiltration depths of MSPs were investigated in two parts: (i) infiltration of printed powder constructs with Sil25 under different conditions; (ii) infiltration of identical constructs with Promax-10 and Matrix M-3428.

Infiltration of powdered cubes with Sil-25 MSP under different conditions

A set of 30 powder cubes measuring 20x20x20 mm were printed using the full colour printing capability of a Z-Corp Z510 3D colour printer, biocompatible powder and ZBTM58 aqueous binder. A two-part addition-curing MSP (Sil-25 Silicone Elastomer, Abacus, UK; 10:1 by weight) was hand mixed in a plastic container. The cubes were then submerged in the polymer mixture and left under atmospheric air pressure at room temperature for a scheduled time. Cubes were removed from the container after 5 min (n=6), 10 min (n=6), 15 min (n=6), 20 min (n=6) and 25 min (n=6), and then left for 24 h on a glass slab to allow drainage of the residual silicone and to complete setting. Following infiltration, the cubes were bisected equally using a No. 11 scalpel blade. The internal aspects of the cubes were then stained using cochineal dye which was effective in colouring the non-infiltrated areas of the blocks, in order to highlight and facilitate measurement of the silicone infiltrated/non-infiltrated boundary (Figure 2).

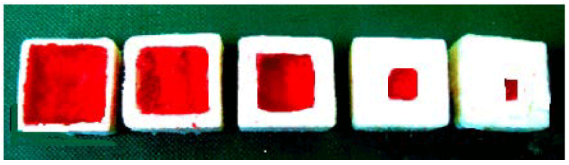

Figure 2: Sectional blocks showing the staining due to the dye and identifying the extent of silicone polymer infiltration. The dye is taken up by the hydrophilic starch, whereas the infiltrated area is hydrophobic and does not take up the dye.

The bisected cubes were then orientated under a travelling microscope (Mitutoyo TM) with X-Y coordinates (Figure 3A). Twelve measurements (three on each cut face of the cube) were taken on either of the two halves of the cubes (Figure 3B), thus a total of 72 measurements were taken for each time period.

The same study was repeated under 2 and 3 bar pressure with two further sets of 30 powder cubes utilised. The infiltration process was carried out in a dental pressure bath under either 2 or 3 bar pressure for time periods identical to those used with the first group.

Infiltration of powdered cubes with Promax-10 and matrix M-3428 MSPs

In this part of the study, two other MSPs were investigated: Promax-10 (Slow Platinum 1:1 Silicone Elastomer, Abacus, UK) and Matrix M-3428 (Platinum 10:1 Silicone Elastomer, Abacus, UK) were infiltrated inside the 20x20x20 mm powdered cubes. The infiltration process was performed under 3 bar pressure over at identical time intervals.

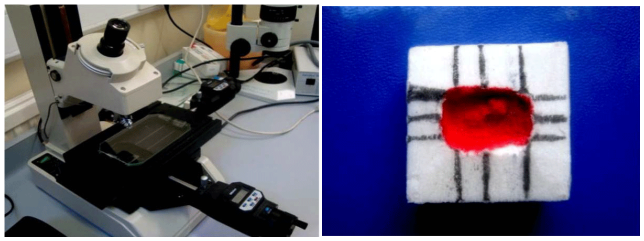

Figure 3: Twelve measurements of infiltration depth were undertaken on each block (A) using a travelling microscope (Mitutoyo TM) with X-Y coordinates (B).

Silicone/powder ratio by weight

The percentage of each component (biocompatible powder and the MSP) was determined by weight in the final models. Eight powder blocks (45x45x4mm) were printed using the Z510 printer and weighed using a sensitive digital balance (Mettler AJ100). The blocks were then infiltrated with Sil-25 under 3 bar pressure for 25 min and left for 24 h. The infiltrated blocks were then weighed to estimate the percentage of each component within the fully infiltrated blocks.

Scanning electron microscopy analysis

Printed blocks were infiltrated with Sil-25, Promax-10 and Matrix M-3428, and slides prepared in order to examine the quality of the infiltration of the MSP inside the printed constructs using scanning electron microscopy (SEM). In addition, SEM analysis was performed for a hand-mixed composite of 40% biocompatible powder and 60% Sil-25 MSP by weight. The two components were mixed until a homogenous mixture was achieved. The mixture was then poured into a 45x45x4mm stainless steel mould, pressed and left at room temperature for 24 h. After setting was complete, the block was cut into thin slices with a surgical blade for SEM analysis.

Statistical analysis

Statistical analysis was carried out to compare the infiltration depths between the different groups and their parameters – time, pressure and different MSP's. Between-group comparisons were made using two-way ANOVA with Tukey's HSD (PASW Statistics 18, SPSS Inc).

Results

Dye coloration in the non-infiltrated areas of the blocks clearly defined the areas that were and were not infiltrated with the silicone polymer. Infiltration of the powder cubes by silicone polymer can be clearly seen in Figure 2. The mean infiltration depth of Sil-25 MSP into the powder cubes under normal atmospheric pressure, and under 2 and 3 bar pressure is shown in Table 1.

Under atmospheric pressure, the depth of infiltration remained at approximately 1 mm and was not affected by the length of time of the infiltration process. However the application of 2 and 3 bar pressure increased the penetration depth significantly; after 20-25 min the depth of penetration was in the order of 4 mm and 8 mm respectively.

Figure 4 illustrates graphically the effects of time and pressure on the depth of infiltration of Sil-25 into the powder cubes. Applying pressure had a significant effect on the degree of infiltration into the powder constructs. Two-way ANOVA revealed a significant difference ($p<0.05$) in the infiltration depths between the 3 groups – under atmospheric pressure, 2 bars and 3 bars.

		Infiltration depth (mm)				
Infiltration time		5 min	10 min	15 min	20 min	25 min
MSP	Pressure					
Sil-25	1 bar	0.94 (0.08)	1.19 (0.10)	1.16 (0.05)	1.27 (0.13)	1.35 (0.08)
Sil-25	2 bar	1.99 (0.10)	2.76 (0.23)	3.30 (0.28)	3.75 (0.19)	3.88 (0.17)
Sil-25	3 bar	3.94 (0.15)	5.43 (0.20)	6.36 (0.51)	7.71 (0.27)	8.65 (0.49)
Promax-10	3 bar	1.87 (0.20)	2.11 (0.34)	2.14 (0.12)	2.21 (0.17)	2.43 (0.29)
M-3428	3 bar	1.36 (0.13)	2.83 (0.23)	3.15 (0.31)	6.60 (0.21)	7.47 (0.26)

Table 1: Summary of infiltration depth of maxillofacial silicone polymers (MSPs) into 3D printed 20-mm starch cubes: effect of pressure and time.

Data are mean (SD) of 6 replicates

MSP: Maxillofacial Silicone Polymer

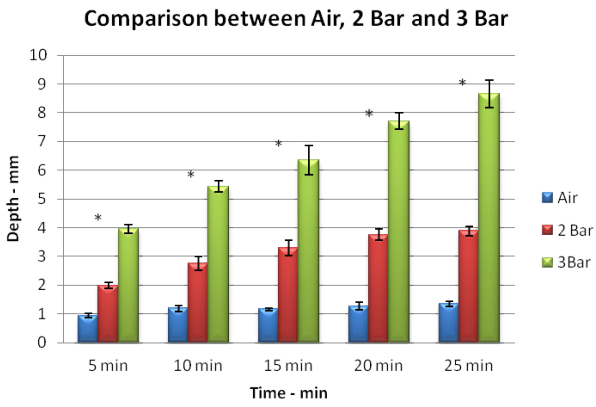

Figure 4: Effect of time and pressure on the infiltration depth of Sil-25 into 20-mm starch cubes (n=6 cubes per time/pressure point). *Indicates significant differences.

The depths of infiltration of the two other MSPs (Promax-10 and Matrix- M3428) inside the powder cubes were investigated under 3 bar pressure, and compared to that of the Sil-25 silicone polymer (Table 1 and Figure 5).

It can be seen that Sil-25 penetrated deeper than Promax10 and M-3428. A maximum of 8.65 mm was recorded for Sil-25 at 3 bar pressure after 25 min, compared with 2.43 mm and 7.47 mm for Promax-10 and M-3428, respectively, under identical conditions. Tukey's HSD test revealed a significant difference ($p<0.05$) in the

infiltration depth between the three silicone polymers for the scheduled times. Results also illustrate that there was no notable increase in the penetration depths of Promax-10 over time under the same conditions as were applied to M-3428 and Sil-25. In contrast, after 20 min and 25 min the infiltration depth of M3428 MSP was comparable to that of Sil-25 MSP.

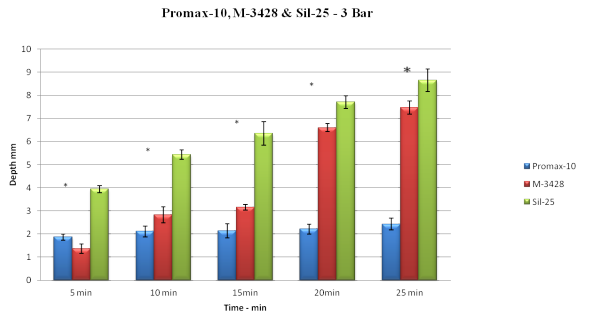

Figure 5: Comparison of infiltration depth into 20-mm starch cubes between Sil-25, M-3428 and Promax-10 at 3 bar (n=6 cubes per time/pressure point). *Indicates significant differences.

Silicone/starch ratio by weight

The mean weight (SD) of the powder blocks was 3.50 (0.04) g. Twenty-four hours after infiltration with Sil25 for 25 min at 3 bar pressure, the mean weight (SD) of the fully infiltrated blocks was 8.50 (0.07) g. Thus, the biocompatible powder comprises approximately 40% of the total weight, whereas the MSP amounts to 60% of the fully infiltrated blocks.

SEM interpretation

SEM analysis of the infiltrated powder blocks showed amorphous, non-crystalline shaped particles with an associated variation in particle sizes. These particles appeared to be randomly orientated and showed a loosely packed arrangement, with a small amount of spacing in between (Figure 6A).

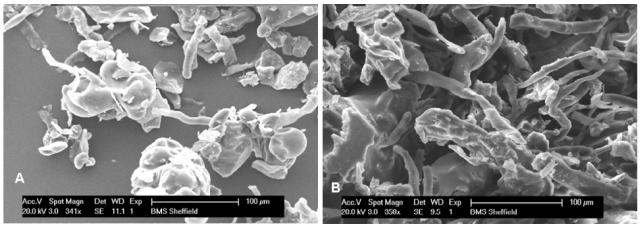

Figure 6: SEM images of (A) starch particles (x341), (B) Starch infiltrated Sil-25 (x358).

SEM further indicated that there was a relatively disorganized distribution of powder particles within the silicone infiltrate which was revealed as spaces and gaps. SEM images of Sil-25 infiltrated inside blocks subjected to 3 bar pressure are shown in Figure 6B. However as Figure 7A demonstrates, SEM analysis of 40% by weight biocompatible powder incorporated into 60% by weight Sil-25 SP by hand mixing revealed a more homogeneous and coherent distribution of the powder and SP with fewer gaps and spaces in between particles. Higher magnification revealed narrow gaps and spaces around the starch particles indicating a lack of integration or solubility between the powder particles and the SP (Figure 7B). Similar results were also found for the other MSPs.

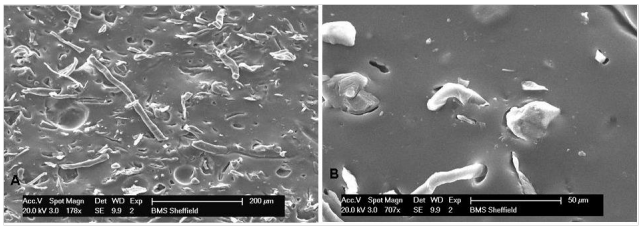

Figure 7: (A) SEM image of Sil-25 hand-mixed with 40% starch by weight (x178). (B) Higher magnification showing spaces around the starch particles (x707).

Discussion

Penetration of the infiltrant inside the printed cubes was determined by the time and pressure to which the samples were subjected, and by the curing rates of the polymers used as infiltrants. The infiltration depths of three different SPs: Sil-25, Promax-10 and M-3428, inside the powder cubes were evaluated to explore whether infiltrants with different physical properties have a differential effect on the depth of penetration. Furthermore, a range of pressures and time frames were applied to assess how these parameters relate to penetration depth inside the powder cubes. The objective was to investigate whether the infiltration depth could be influenced by different conditions including type of the infiltrant used, time and pressure.

The data obtained clearly show that the use of ambient air pressure has no real influence on the penetration depth of MSPs into 3D printed cubes. This is probably due to the relatively high viscosity of the MSPs used and the increased likelihood that the binder on the external surfaces of the printed blocks acted as a barrier to the flow of the polymers inside the blocks. It was therefore predicted that an increase in pressure was required in order to improve the depth and rate of infiltration. The results showed clearly that the use of pressure had a very positive influence on the depth of penetration of the MSPs, whereas time alone was insufficient to allow the MSP to infiltrate deep inside the 3D printed cubes. It was also observed that printing with resin bound powder produces softer and more flexible parts after infiltration with MSP and thus these appear to be more suitable for producing soft tissue prostheses.

These data showed that pressure had a significant impact on the penetration depth. When the infiltration process was performed at 2 and 3 bar pressure, the penetration of the MSP increased considerably. However, the penetration depth of the MSP under 2 bar pressure was less than at 3 bar pressure. This indicates that higher infiltration depths can be achieved by increasing the pressure applied. Since the items printed can be infiltrated from all sides, this would suggest that under these conditions, the maximum total depth of infiltration possible for a prosthesis would be approximately 16 mm. Therefore, as long as the prosthesis was no more than 16 mm thick, full penetration with Sil-25 and Matrix M-3428 SPs could be achieved. It can also be

reasonably argued that a depth of penetration of 10-12 mm would be more than adequate for most applications for this project.

When comparing the depth of penetration of Sil-25, Matrix M-3428 and Promax-10 into the powder cubes, the data showed that Sil-25 and M-3428 were significantly more effective in penetrating the cubes when compared to Promax-10. These differences can be attributed to the setting time and viscosity of the different MSPs. Promax-10 has a quicker setting time and therefore becomes more viscous within a shorter period of time after mixing both silicone components. In other words, Promax-10 has a shorter working time than Sil-25 and M-3428 in order to permit penetration of the SP inside the printed constructs. The infiltration process slows down when the viscosity starts to increase as part of the normal setting reaction.

Although in the second part of the study a maximum infiltration depth of 8 mm was achieved, it was unclear how consistent or homogeneous this infiltration was. The SEM analysis was undertaken to answer this specific question. Macroscopically, the samples appeared to be fully infiltrated and smooth. However, under SEM the infiltrated blocks showed evidence of porosity that resembled patches or small spaces within a confluent albeit textured base (Figure 6B). This may be related to the viscosity of the silicone polymer used and/or wettability factors of the individual constituents. Silicone polymers generally have a low surface-free energy and are considered to be hydrophobic [18], whilst the biocompatible powder used was relatively hydrophilic. Unfilled patches can potentially occur when air is trapped in the central part of the cubes after the SP starts to penetrate inside from all aspects under the effect of pressure. These factors may explain the reduced homogeneity and coherence between the MSP and the powder particles, as shown in Figure 6B. This magnified image for mixed particles and MSP shows gaps around each particle, which indicates a lack of interaction and coherence between the powder particles and the polymers, even when the two components appear to be mixed adequately. This phenomenon is attributed to the hydrophobic nature of the MSP's [19], and this influences the general properties of the final product. Figure 7A shows a more homogeneous distribution of the powder inside the SP, with fewer voids shown after hand mixing of both components compared to the silicone infiltrated powder samples (Figure 6B). This probably occurs because the printed samples are sealed from outside by the binder, which acts as a potential albeit weak barrier for infiltration of the SP inside the printed blocks.

Conclusions

Pressure has a significant impact on the infiltration rate of rubber silicone elastomer into 3D printed powder objects. Therefore, the depth of penetration of Sil-25 and Matrix M-3428 into printed constructs under 3 bar pressure is sufficient for prostheses that are less than 16 mm thick. Promax-10 was considered a relatively poor infiltrant compared to the other two MSPs. Furthermore, SEM revealed the presence of small voids and pores within the infiltrated areas although the effect of these on the macroscopic properties is yet unknown.

Acknowledgement

This study was supported in part by a Wellcome Trust Translational Research Grant awarded to Professor J M Yates and Fripp Design Limited, UK. Faraedon Zardawi acknowledges the Iraqi Ministry of Higher Education and Scientific Researches for their sponsorship of this Doctoral Scholarship which led to the completion of this report.

References

1. Khan Z, Gettleman L, Jacobson CS (1992) Conference report: materials research in maxillofacial prosthetics. J Dent Res 71: 1541-1542.
2. Leonardi A, Buonaccorsi S, Pellacchia V, Moricca LM, Indrizzi E, et al. (2008) Maxillofacial prosthetic rehabilitation using extraoral implants. J Craniofac Surg 19: 398-405.
3. Valauri AJ (1982) Maxillofacial prosthetics. Aesthetic Plast Surg 6: 159-164.
4. Cheah CM, Chua CK, Tan KH (2003) Integration of laser surface digitizing with CAD/CAM techniques for developing facial prostheses. Part 2: Development of molding techniques for casting prosthetic parts. Int J Prosthodont 16: 543-548.
5. Cheah CM, Chua CK, Tan KH, Teo CK (2003) Integration of laser surface digitizing with CAD/CAM techniques for developing facial prostheses. Part 1: Design and fabrication of prosthesis replicas. Int J Prosthodont 16: 435-441.
6. Dimitrov D, Schreve K, De Beer N (2006) Advances in three dimensional printing–state of the art and future perspectives. Rapid Prototyping Journal, 2006; 12:136-147.
7. Carrion A (1997) Technology forecast on ink-jet head technology applications in rapid prototyping. Rapid Prototyping Journal 3: 99-115.
8. Jiao T, Zhang F, Huang X, Wang C (2004) Design and fabrication of auricular prostheses by CAD/CAM system. Int J Prosthodont 17: 460-463.
9. Coward TJ, Scott BJJ, Watson RM, Richards R. A (2006) Comparison between computerized tomography, magnetic resonance imaging, and laser scanning for capturing 3-dimensional data from a natural ear to aid rehabilitation. Int J Prosthodont 19: 92-100.
10. Coward TJ, Watson RM, Wilkinson IC (1999) Fabrication of a wax ear by rapid-process modeling using stereolithography. Int J Prosthodont 12: 20-27.
11. Nusinov NS, Gay WD (1980) A method for obtaining the reverse image of an ear. J Prosthet Dent 44: 68-71.
12. Mankovich NJ, Curtis DA, Kagawa T, Beumer J 3rd (1986) Comparison of computer-based fabrication of alloplastic cranial implants with conventional techniques. J Prosthet Dent 55: 606-609.
13. Ciocca L, De Crescenzio F, Fantini M, Scotti R (2010) CAD/CAM bilateral ear prostheses construction for Treacher Collins syndrome patients using laser scanning and rapid prototyping. Comput Methods Biomech Biomed Engin 13: 379-386.
14. Ciocca L, Mingucci R, Gassino G, Scotti R (2007) CAD/CAM ear model and virtual construction of the mold. J Prosthet Dent 98: 339-343.
15. Eggbeer D, Bibb R, Evans P, Ji L (2012) Evaluation of direct and indirect additive manufacture of maxillofacial prostheses. Proc Inst Mech Eng H 226: 718-728.
16. Gatto M, Memoli G, Shaw A, Sadhoo N, Gelat P, et al. (2012) Three-dimensional printing (3DP) of neonatal head phantom for ultrasound: thermocouple embedding and simulation of bone. Med Eng Phys 34: 929-937.
17. van Noort R (2012) The future of dental devices is digital. Dent Mater 28: 3-12.
18. Waters MG1, Jagger RG, Polyzois GL (1999) Wettability of silicone rubber maxillofacial prosthetic materials. J Prosthet Dent 81: 439-443.
19. Jayasekara R, Harding I, Bowater I, Christie GBY , Lonergan GT (2004) Preparation, surface modification and characterisation of solution cast starch PVA blended films. Polym Test 23: 17-27.